Fabrication and Mechanical Behavior of Al_2O_3/TiC/Ni Graded Laminates with Surface Compressive Stresses†

Junshan LIN* and Yoshinari MIYAMOTO**

Abstract

Symmetrically graded laminates of the Al_2O_3/TiC/Ni/TiC/Al_2O_3 were fabricated by SHS/HIP process. Compressive residual stresses as high as 100~300 MPa were introduced into the outer Al_2O_3 layers by utilizing the thermal expansion mismatch between the outer and inner layers. The effect of the surface compressive residual stress on the strength and toughness of Al_2O_3 was evaluated by three point bending tests and the Vicker's indentation method. The results showed that the surface compressive stress can effectively improve the strength and toughness of the ceramic laminates.

KEY WORDS (functionally graded materials) (residual stress) (fracture toughness)

1. Introduction

Various methods to modify the brittle nature of ceramics have been developed. For instance, *in situ* formation of large elongated grains in monolithic Si_3N_4 can raise the fracture toughness to a level of 8~12 MPa·$m^{1/2}$ [1]. Incorporation of silicon carbide, carbon or tyranno fibers into the ceramic matrix can produce a toughness of 20~35 MPa·$m^{1/2}$ [2]. The toughening mechanism is mainly attributed to the crack bridging of elongated grains or fibers. Transformation toughening of Ce doped TZP results in a high toughness ranging from 10 to 18 MPa·$m^{1/2}$ [3]. These ceramics are known to show R-curve behavior, i.e., the fracture resistance increases with the crack growth[4].

Another useful way is to introduce a compressive residual stress into the ceramics. Such stress can depress tensile stress, prevent crack initiation and modify the brittle nature of ceramics. A typical example is tempered or ion-exchanged glass, in which the residual compressive stress is induced at the surface. Lange[5] and Green[6] introduced a compressive stress in ceramics by utilizing the volume expansion accompanying the phase transformation of ZrO_2. However, these methods are limited since the depth of the compressive stress is only a few tens of microns. Virker and co-workers[7-9] fabricated a trilaminate structure with a deep compressive stress which was developed by the mismatch of the thermal expansion between the inner and outer layers. By selecting the appropriate structure and composition of every layer, such trilaminate structures enable the material to have a wide range of compressive stresses in both the depth and the magnitude.

In this study, a graded structure in the system of Al_2O_3/TiC/Ni was fabricated by a self-propagating high-temperature synthesis-aided hot isostatic pressing (SHS/HIP) process. The microstructures of the sintered specimen were analysed by SEM. The residual stress and mechanical properties were evaluated experimentally and analytically.

2. Experimental Procedure

The compositions of the outer, intermediate and central layers are Al_2O_3+0.8wt%MgO, TiC+45wt%Al_2O_3+5 wt%Ni, and TiC+30wt%Ni+10wt%Mo_2C, respective-ly. A cylindrical die was symmetrically packed with above powders to form the green body. After cold isostatic pressing at 200 MPa, the green body was vacuum sealed into a borosilicate glass capsule with a BN powder bed, then placed into a graphite chemical oven as shown in **Figure 1**. The encapsulated green body was embedded in a low cost silicon powder which was used as a fuel for instantaneous heating. In this experiment, 40 gram of silicon powder was added.

Figure 2 shows the schematic diagram of the SHS/HIP process. In HIP, after holding at 780°C for 20 minutes when the glass capsule became soft, the nitrogen pressure was increased up to 100 MPa, then the chemical oven was heated to 1150°C. During the period of heating, the silicon powder was ignited by the exothermic reaction of the thermite pellets at about 1030°C. The highest temperature the chemical oven could reach was 2100°C

† Received on June 1, 1998
* Post Doctral Research Fellow
** Professor of Osaka University

Transactions of JWRI is published by Joining and Welding Research Institute of Osaka University, Ibaraki, Osaka 567-0047, Japan.

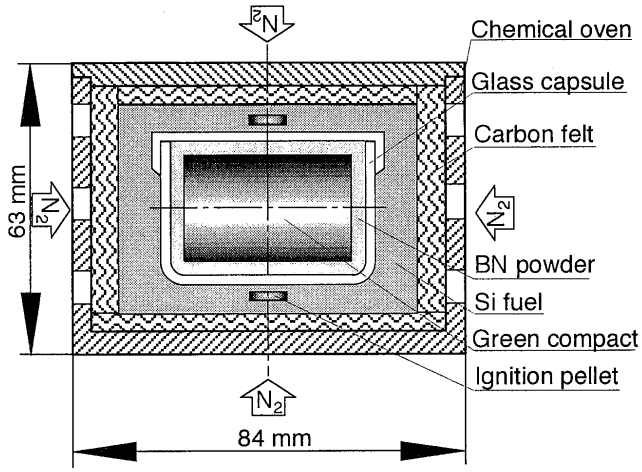

Fig. 1 Schematic diagram of the chemical oven used in SHS/HIP sintering.

because of the reaction heat of silicon nitriding. The samples were held at the temperature of 1150°C for 30 minutes and then cooled in the furnace.

The geometry of the pre-designed sample was a five-layer cylindrical disk with a diameter of 30 mm, and thickness of 5~7 mm. All samples had the same thickness in the central layer (2 mm) and intermediate layer (1 mm), but had different thicknesses in the outer layers. They were 0.5 mm, 1.0 mm and 1.5 mm, and denoted as FGM(0.5), FGM(1.0) and FGM(1.5), respectively. Monolithic Al_2O_3 was also prepared in the same SHS/HIP process for comparing with graded materials.

After the samples were polished to a diamond surface finish of 3 μm, the residual stress at the surface of Al_2O_3 layer was measured by an X-ray diffraction method.

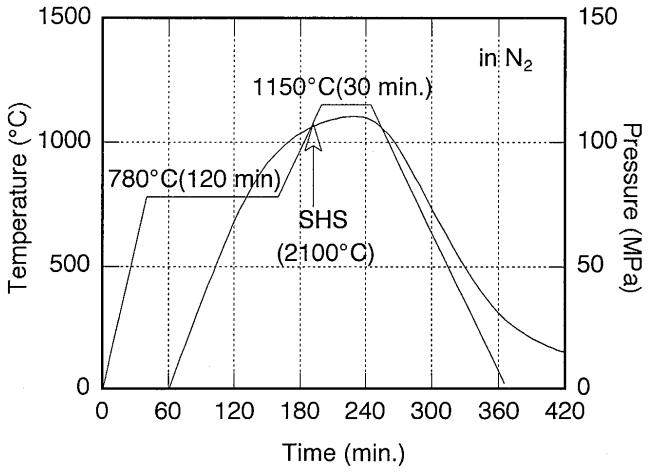

Fig. 2 SHS/HIP Sintering process.

Young's modulus and Poison's ratio of Al_2O_3 used for the analysis were 400 GPa and 0.23, respectively. Vicker's hardness and indentation fracture toughness were measured at the Al_2O_3 surface and the cross section of samples with an indentation load up to 196N. Compositional profiles were analyzed on the cross section by using EDX. Microstructure was observed by scanning electron microscopy. Three-point bending tests were conducted at room temperature for specimens cut into bars with the size of $2\times(5\sim7)\times23$ mm^3. The indentation strength tests were carried out for the specimens indented at the center of tensile surface. Three specimens were provided for each bending test.

3. Results and Discussion

3.1 Structure and residual stress analyses

The samples sintered by SHS/HIP process were almost completely densified. The volume shrinkage was ~40%. **Figure 3** shows SEM photographs of the fractured surface from the outer layer to the central layer. The outer layer consists of Al_2O_3 grains of 2~3 μm in size as seen in photo (a). The addition of MgO effectively restrained the anomalous growth of the Al_2O_3 grains. Photo (b) shows the interfacial region between the outer and intermediate layers. Photo (c) is the intermediate layer, which consists of fine grains (below 1~2 μm) of Al_2O_3 and TiC. Photo (d) is the interfacial region between the intermediate and central layers. Photo (e) is the central layer, where Mo_2C additives also take effect in restraining the growth of the TiC grains.

Figure 4 shows the composition profile of the FGM(1.0). The outer layer only showed Al_2O_3 phase. The Ni content was about 28 wt% at the central layer, which decreased gradually towards the outer Al_2O_3 layer. Though nickel was usually molten during SHS/HIP, no Ni penetration into the Al_2O_3 layer was observed. This is probably due to the poor wettability between Al_2O_3 and Ni[10].

The residual stresses of FGM(1.0) determined by X-ray diffraction are shown in **Figure 5**. It was approximately 220 MPa at the center of the outer Al_2O_3 layer, and decreased gradually toward the periphery. This stress is believed to be induced by the thermal expansion mismatch between the outer and inner layers. Based on an elastic model and beam theory, the residual stress can be estimated by assuming a simple trilaminate structure as follows:

$$\sigma_R = -\frac{E_1 E_2 \Delta\alpha \Delta T}{(1-\nu)\left[E_2 + 2E_1(t_1/t_2)\right]} \quad (1)$$

where $\Delta\alpha$ is the difference of thermal expansion coefficients between the outer and inner layers. ΔT is the

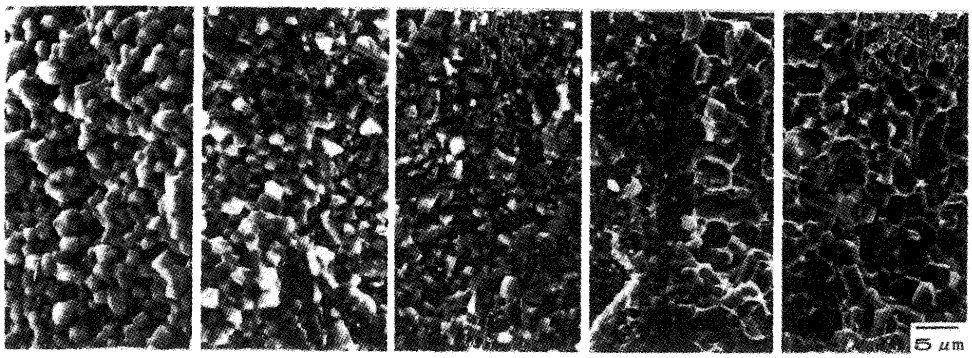

(a) (b) (c) (d) (e)

Fig. 3 Fractured surface of the material FGM(1.0). (a) outer Al_2O_3 layer, (b) interfacial region of Al_2O_3/(Al_2O_3-TiC) layers, (c) intermediate (Al_2O_3-TiC) layer, (d) interfacial region of (Al_2O_3-TiC)/(TiC-Ni) layers, (e) central (TiC-Ni) layer.

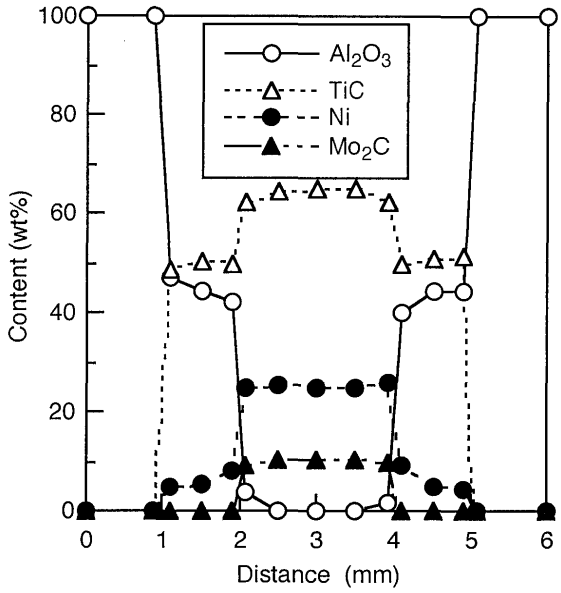

Fig. 4 Composition profiles of the material FGM(1.0).

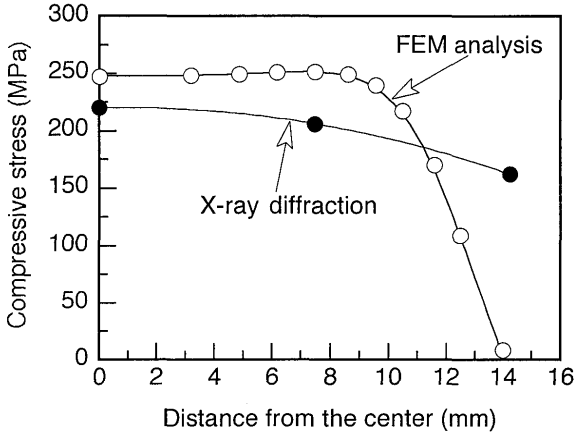

Fig. 5 Profile of residual compressive stress from the center to the peripheral region on the outer Al_2O_3layer of FGM(1.0).

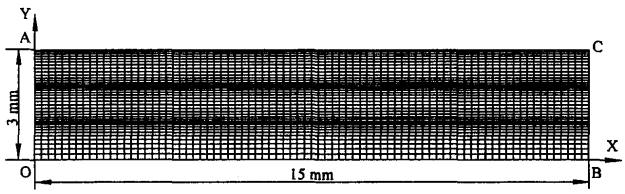

Fig. 6 FEM meshes used for the calculation of the residual stress.

temperature drop from the sintering temperature. Young's modulii and Poisson's ratios are assumed to be uniform through the material for simplicity and equal to the values of Al_2O_3, E=400 GPa and ν=0.23, respectively. t_1, t_2 are thicknesses of the outer and inner layers. A dilatometer was used to measure the mean thermal expansion coefficient of the inner layer up to 1000°C, and was found to be ~8.8×10^{-6}/°C. For the Al_2O_3, the reported value is 8.2×10^{-6}/°C[11]. With the temperature drop assumed to be ~1150 °C, the residual stress σ_R was calculated to be -230 MPa for t_1=1 mm and t_2=4 mm.

Based on the model as shown in **Figure 6**, the distribution of the residual stress at the surface layer was calculated by the finite element method (FEM). The results are illustrated in Figure 5 as well. It can be seen that the FEM results are consistent with the X-ray diffraction results except at the edge part.

The good correlation between the calculated and observed stresses suggested that the residual stress was mainly induced by the thermal expansion mismatch in the laminar structure. Other contributions such as sintering tensile stress in the inner layer was estimated to be over

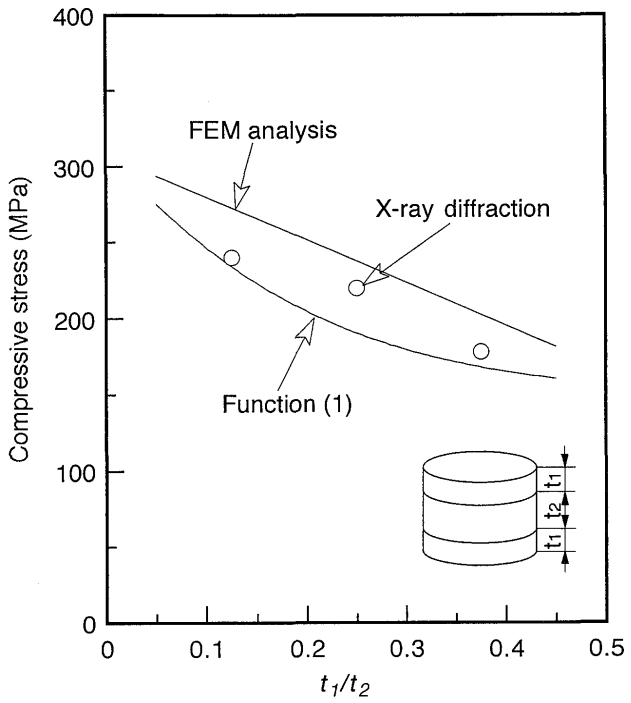

Fig. 7 Residual stress in the outer Al_2O_3 layer as a function of thickness ratio of the outer/inner layers.

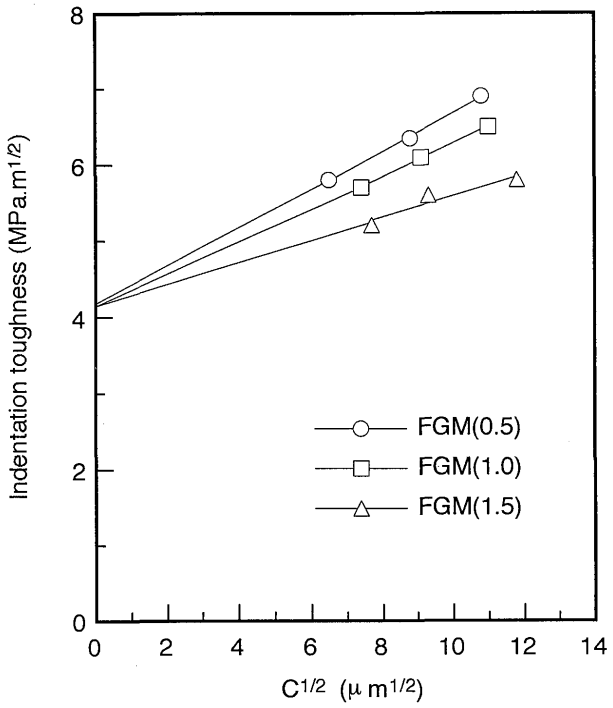

Fig. 8 K_C at the center of the surface Al_2O_3 layer vs crack length $C^{1/2}$.

100 MPa using the relation of stress balance between the outer and inner layers.

Figure 7 shows the residual stress in the outer Al_2O_3 layer as a function of the thickness ratio of outer/inner layers. As expected, the compressive residual stress in the outer layer increases with a decrease in the thickness ratio of outer layer to inner layer. The residual stresses determined by X-ray diffraction are consistent with the theoretical curves from equation (1) and FEM analysis. These results show that the residual stress in graded materials obeys the mechanism of the internal stress balance associated with the thickness ratio of the outer/inner layers.

3.2 Mechanical properties

According to the indentation fracture mechanics for the half penny-shaped flaw [9, 12], the indentation toughness, K_C, is related to the indentation crack length c by the following expression:

$$K_C = \chi \frac{P}{c^{3/2}} + \frac{2}{\sqrt{\pi}} \sigma_R \sqrt{c} \qquad (2)$$

where χ is a constant, P the indentation load and σ_R the residual stress. The first term, $\chi \frac{P}{c^{3/2}}$, is the intrinsic toughness in the state free of residual stress, denoted as K_0 later. K_C and $\sqrt{c}$ follow a linear relation associated with K_0 and σ_R.

Figure 8 plots the K_C measured at the center of Al_2O_3 surface against $\sqrt{c}$. The residual stresses derived from the tangent of each solid line using equation (2) were -240, -220, -180 MPa for the materials FGM(0.5), FGM(1.0) and FGM(1.5), respectively. The good agreement between X-ray stress analysis and the mechanical analysis indicates that the toughening of the Al_2O_3 layer is entirely due to the compressive residual stress produced by thermal expansion mismatch.

Figure 9 shows the profiles of Vicker's hardness Hv and toughness K_C at the surface of the cross section of material FGM(1.0). The hardness was 20 GPa at the surface Al_2O_3, which was slightly higher than that of the monolithic Al_2O_3 (18 GPa). It decreased to 11 GPa at the Ni rich central layer. The toughness was 6 $MPa \cdot m^{1/2}$ at the surface Al_2O_3, increased to 8 $MPa \cdot m^{1/2}$ at the intermediate layer and 15 $MPa \cdot m^{1/2}$ at the central layer due to the addition of metal Ni. The fracture toughness of the monolithic Al_2O_3 was 4 $MPa \cdot m^{1/2}$.

Figure 10 shows the relationship of the indentation bending strength versus indentation load for the material FGM(1.0) and monolithic Al_2O_3. It is noted that the flexural strengths of the graded material were higher than the monolithic Al_2O_3 at every indentation load of 4.9~196.0 N, especially at the loads lower than 9.8 N. This means that the damage tolerance of the Al_2O_3 was enhanced by a graded structure with surface compressive stress. **Figure**

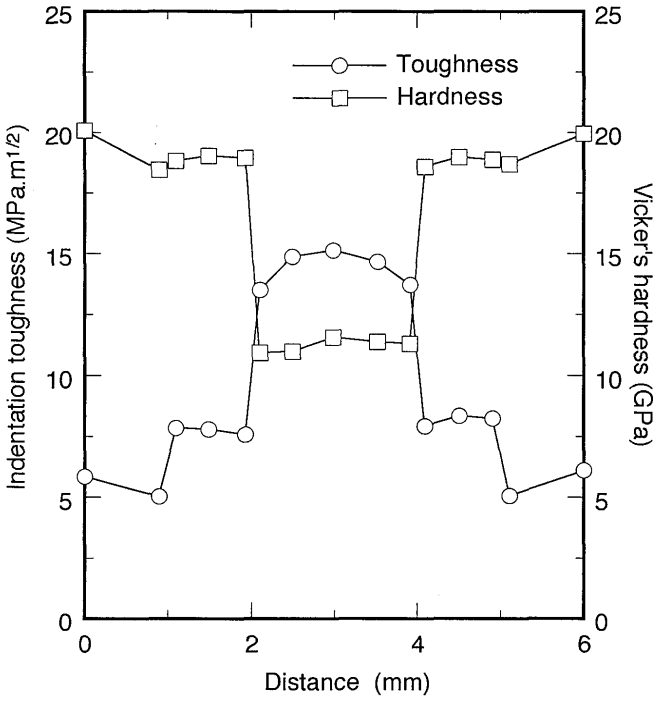

Fig. 9 Profiles of hardness, H_V, and toughness K_C, measured on the cross section of the material FGM(1.0).

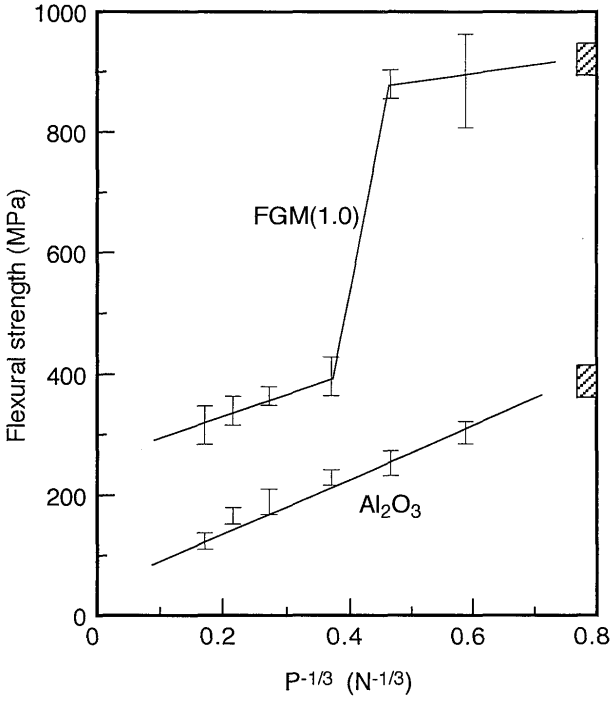

Fig. 10 Flexural strength vs indentation load for the material FGM(1.0) and monolithic Al_2O_3.

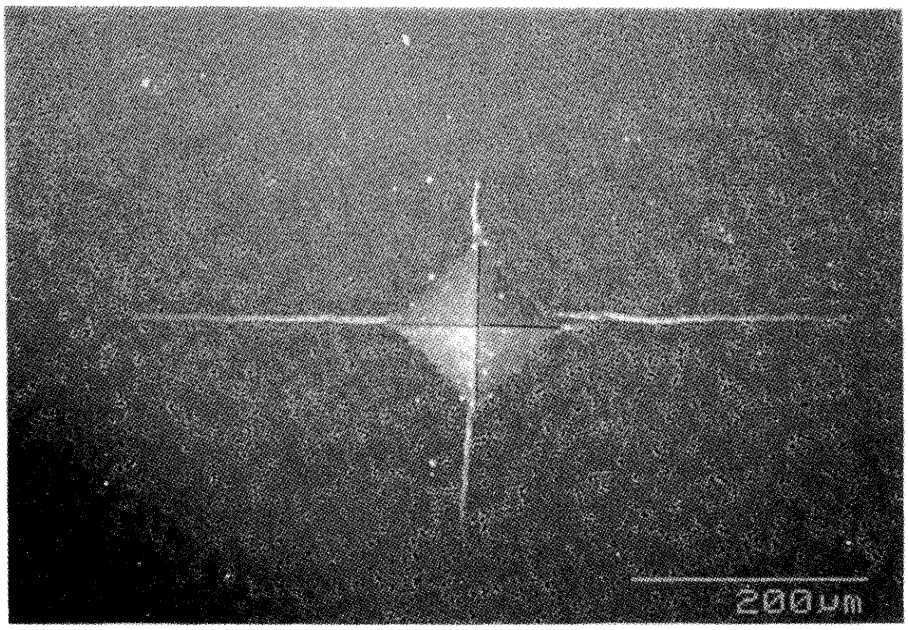

Fig. 11 Cracks induced by indentation (indentation load: 196 N).

11 shows an indentation made on the tensile side of a test bar. It can be seen that the indentation induced longer cracks in the length direction than in the width direction because of the stress relaxation along the width direction after the test bar was cut out. But the indentation strength depends on the cracks in the width direction. Because of the constraint effect of the high compressive residual stress in the length direction, the half-penny shape crack could not be developed in the width direction at low indentation load, and the residual stress relaxation induced by the indentation crack almost did not occur. With increasing indentation load, however, the half-penny shape crack was formed, and led to the relaxation of the residual stress. Thus the strengthening effect of the compressive stress was weakened, as seen in Figure 10, when the indentation load was higher than 9.8 N.

The fractography suggested that the fracture origin existed at the Al_2O_3 surface when the indentation load was over 19.6 N, but it changed to the interfacial region between the outer Al_2O_3 layer and the intermediate layer when below 9.8 N. This also suggested that the maximum tensile stress, which was a sum of bending stress and the residual stress, was not located at the surface as usual in flexural tests, but at the interior region, i.e., the stress relaxation induced by indentation almost did not occur.

4. Conclusions

The SHS/HIP process is a unique process which can rapidly consolidate such heterogeneous materials. Symmetrically graded structures can effectively control the internal stress of ceramics by tailoring the mismatch of the thermal expansion of changing the geometry of the specimen.

For graded laminates of the Al_2O_3/TiC/Ni/TiC/Al_2O_3 type, a strong compressive residual stress, as high as 200~300 MPa, can be introduced into the outer Al_2O_3 layer and controlled by changing the thickness of the surface layer. Both the strength and the toughness of the materials increase with increasing compressive surface stress.

References

1) C. W. LI and J. YAMANIS
Super-Tough Silicon Nitride with R-Curve Behavior,
Ceram. Eng. Sci. Proc., 10-7 (1989), 632-645.

2) R. NASLAIN and F. LANGLAIS
CVD-Processing of Ceramic-Ceramic Composite Materials,
Proceedings of Twenty-First University Conference on Ceramic Science, Pennsylvania, June (1986), 145-146.

3) K. TSUKUMA and M. SHIMADA
Strength, Fracture Toughness and Vickers Hardness of CeO_2 Polycrystals (Ce-TZP),
J. Mater. Sci., 20-4 (1985), 1178-1184.

4) M. P. HARMER, H. M. CHEN and G. A. MILLER
Unique Opportunities for Microstructural Engineering with Duplex and Laminar Ceramic Composites,
J. Amer. Ceram. Soc., 75-7 (1992), 17151728.

5) F. F. LANGE
Compressive Surface Stresses Developed in Ceramics by an Oxidation-Induced Phase Change,
J. Amer. Ceram. Soc., 63-1 (1980), 38-40.

6) D. J. GREEN
A Technique for Introducing Surface Compression into Zirconia Ceramics,
J. Amer. Ceram. Soc., 66(1983), C178-179.

7) A. V. VIRKAR, J. L. HUANG and R. A. CUTLER
Strengthening of Oxide Ceramics by Transformation-Induced Stresses,
J. Amer. Ceram. Soc., 70-3 (1987), 164-170.

8) A. V. VIRKAR, J. F. JUE, J. J. HANSEN and R. A. CUTLER
Mesurement of Residual Stresses in Oxide-ZrO_2 Three-Layer Composites,
J. Amer. Ceram. Soc., 71-3 (1988), C148-151.

9) R. SATHYAMOORTHY, A. V. VIRKAR and R. A. CUTLER
Damage-Resistant SiC-AlN Layered Composites with Surface Compressive Stresses,
J. Amer. Ceram. Soc., 75-5 (1992), 1136-1141.

10) J. E. MCDONALD and J. G. EBERHART
Adhesion in Aluminum Oxide-Metal Systems,
Transactions of the Metallurgical Society of AIME, 233-3 (1965), 512-517.

11) JANAF Thermochemical Table, 1 (1964) 176.

12) D. B. MARSHALL and B. R. LAWN
Residual Effects in Sharp Contact Cracking: I,
J. Mater. Sci. 14-8 (1979), 2001-2012.